Article

Experimental Investigation on the Impact of Drying–Wetting Cycles on the Shrink–Swell Behavior of Clay Loam in Farmland

Wei Qi [1] **, Ce Wang** [2] **, Zhanyu Zhang** [2,*] **, Mingyi Huang** [1] **and Jiahui Xu** [2]

[1] College of Water Conservancy and Hydropower Engineering, Hohai University, Nanjing 210098, China; qiwei@hhu.edu.cn (W.Q.); 20200923@hhu.edu.cn (M.H.)
[2] College of Agricultural Science and Engineering, Hohai University, Nanjing 211100, China; wangce@hhu.edu.cn (C.W.); jiahuixu@hhu.edu.cn (J.X.)
[*] Correspondence: zhanyu@hhu.edu.cn

Abstract: Soil shrink–swell behavior is a common phenomenon in farmland, which usually alters the process of water and solute migration in soil. In this paper, we report on a phenomenological investigation aimed at exploring the impact of drying–wetting cycles on the shrink–swell behavior of soil in farmland. Samples were prepared using clay loam collected from farmland and subjected to four drying–wetting cycles. The vertical deformation of soil was measured by a vernier caliper, and the horizontal deformation was captured by a digital camera and then calculated via an image processing technique. The results showed that the height, equivalent diameter, volume and shrinkage-swelling potential of the soil decreased with the repeated cycles. Irreversible deformation (shrinkage accumulation) was observed during cycles, suggesting that soil cracks might form owing to previous drying rather than current drying. The vertical shrinkage process consisted of two stages: a declining stage and a residual stage, while the horizontal shrinkage process had one more stage, a constant stage at the initial time of drying. The VG-Peng model fit the soil shrinkage curves very well, and all shrinkage curves had four complete shrinkage zones. Drying–wetting cycles had a substantial impact on the soil shrinkage curves, causing significant changes in the distribution of void ratio and moisture ratio in the four zones. However, the impact weakened as the number of cycles increased because the soil structure became more stable. Vertical shrinkage dominated soil deformation at the early stage of drying owing to the effect of gravity, while nearly isotropic shrinkage occurred after entering residual shrinkage. Our study revealed the irreversible deformation and deformation anisotropy of clay loam collected from farmland during drying–wetting cycles and analyzed the shrink–swell behavior during cycles from both macroscopic and microscopic points of view. The results are expected to improve the understanding of the shrink–swell behavior of clay loam and the development of soil desiccation cracks, which will be benefit research on water and solute migration in farmland.

Keywords: drying–wetting cycles; digital image processing; shrink–swell behavior; soil shrinkage curve; soil cracks; irreversible deformation; anisotropy of deformation

1. Introduction

Soil shrinkage and swelling is a common phenomenon in nature, primarily resulting from the dynamic change of soil pore structure, which is macroscopically manifested as soil volume change in response to moisture variation. The soil volume change has an impact on the stability and functionality of soil-based constructions, such as houses, roads, dikes and so on [1]. Soil cracking occurs when the tensile strength between soil aggregates or particles is overcome by the tensile stress developed during shrinkage [2]. The existence of cracks can significantly reduce the mechanical strength of soil [3], potentially resulting in the failure of buildings and earth structures [4,5]. In agriculture, soil volume changes cause a deviation of the measured data of soil water retention from the true values, thereby reducing the

accuracy of measurement and simulation of soil moisture conditions in farmland [1,6]. In addition, soil cracks typically act as preferential paths for water movement and solute transport, decreasing the water and fertilizer use efficiency and increasing the risk of deep percolation and groundwater contamination [7–9]. Consequently, soil shrink–swell behavior has become an extensively investigated subject and has attracted the attention of researchers in multiple fields [10,11].

Over the past decades, considerable research efforts were devoted to the investigation of soil shrink–swell behavior. The coefficient of linear extensibility (COLE) was proposed to quantify soil shrinkage potential by Grossman et al. [12] and is extensively used in related research [13–15]. In general, soil with COLE > 0.09 m m^{-1} is considered to have a very high shrinkage potential [16]. However, due to the limitation of COLE in describing the dynamic deformation of soil, the soil shrinkage curve is now widely employed in describing soil shrinkage characteristics as it provides crucial information on the change in soil volume (void ratio) in relation to soil moisture (moisture ratio). A typical soil shrinkage curve is in the shape of an 'S' and consists of four characterized zones: structural shrinkage, proportional shrinkage, residual shrinkage and zero shrinkage [17]. The structural shrinkage zone results from the water loss in large pores such as root holes, biopores and cracks that cause little or slight changes in soil volume. In the proportional shrinkage zone, water is drained from inter-aggregate pores, causing an equal or proportional decrease in soil volume [18]. In the residual shrinkage zone, air enters intra-aggregate pores, and the decrease in water volume is much more than the decrease in soil volume [19]. Zero shrinkage ranges from the shrinkage limit to the dry endpoint, where the soil volume remains nearly constant despite the water loss [20]. Quite a few models are proposed to fit the soil shrinkage curve and to derive the characteristic points segmenting shrinkage zones easily, including the three straight lines model, XP model, PL model and sigmoid model [18,19,21–23]. Regarding swelling, Estabragh et al. [24] reported that the soil swelling curve was also in the shape of an 'S', while Peng and Horn [17] found that the swelling curve was not clearly sigmoidal and the swelling process only contains two stages: virgin swelling and residual swelling with the separation of the wet-side maximum curvature, and the virgin swelling accounts for 81.2–91.9% of swelling volume in contrast with the residual swelling. This discrepancy was probably due to the difference in soil properties and testing procedures. However, hysteresis in soil volume change between the shrinkage and swelling process was reported in both studies. Soil shrink–swell behavior is closely associated with soil intrinsic properties, including clay content and type [25,26], inorganic carbonate content [16], dry bulk density [27,28], etc. On the other hand, it can also be strongly impacted by a large number of influencing factors from external conditions, such as surcharge pressure [29,30], additives [31,32], pore water chemistry [33], dry intensity [34], the freezing–thawing cycle [35,36] and the drying–wetting cycle [37,38].

In general, soils in farmland are exposed to open air, experiencing diurnal variations and seasonal sunny–rainy weather, and thus undergo drying–wetting cycles. However, studies regarding the effect of drying–wetting cycles on soil shrink–swell behavior mostly concern expansive soils or only focus on crack patterns. There are relatively few studies devoted to investigating the effects of drying–wetting cycles on the shrink–swell behavior of soil in farmland. The shrink–swell behavior of soil in farmland reflects the changes in soil porosity and implies the generation or closure of soil desiccation cracks. The study on this aspect is of great importance for further understanding soil pore structure alternation and water and solute migration and for guiding precision irrigation in agricultural fields. Therefore, the main objective of this study is to uncover the impact of drying–wetting cycles on the shrink–swell behavior of soil in farmland. With the aid of digital image processing techniques, which can improve the accuracy of deformation measurement, this study specifically aims to investigate the evolution of (i) the shrinkage–swelling potential, (ii) vertical and horizontal deformation, (iii) shrinkage curves and shrinkage zones and (iv) anisotropy of deformation of the soil during four drying–wetting cycles.

2. Materials and Methods

2.1. Soil Properties

This study was conducted indoors at the Water-Saving Park of Hohai University in Nanjing, Jiangsu Province, China (31°57′ N, 118°50′ E). This region has a typical subtropical monsoon climate with an average annual precipitation of 1073 mm and mean annual evaporation of around 900 mm [39]. The soil used in this study was taken from the upper 20 cm layer of the farmland, where rice and wheat were alternately planted over the last few years. The soil was clay loam according to the ISSS soil texture classification, containing sand, silt and clay in the proportions of 22.7%, 56.2% and 21.1%. The content of soil organic carbon was 11.7 g kg^{-1}. After loosening by a rotary tiller, the soil was collected from the field, crushed and sieved through a 2 mm aperture screen mesh. Afterwards, it was left to air-dry (the gravimetric soil water content was around 4.0%) under high ventilation conditions before use.

2.2. Experimental Design and Testing Procedure

2.2.1. Sample Preparation

The air-dried soil was uniformly backfilled into three Plexiglas boxes (20 cm × 20 cm × 20 cm) with an average dry bulk density of 1.25 g cm^{-3}. The soil surface was precisely flattened, and the final height of soil was controlled at 10 cm. Then, the soil was saturated with pure water for 48 h. One soil core (diameter was 70 mm, height was 52 mm) was collected from each box by the cutting ring method [40], which was used as a soil sample for the shrink–swell experiment. Thus, a total of three samples were prepared. Expanded volumes of soil samples beyond the cutting rings were removed, and the surface of the soil samples was flattened by a scraper. Before sampling, the inner wall of the cutting rings was coated with vaseline to attenuate the friction effect of the wall in sampling and soil shrinkage [41].

2.2.2. Drying–Wetting Cycles

Following sample preparation, the drying–wetting cycles commenced. The saturated samples were initially oven-dried at 40 °C. During drying, the weights of the samples were recorded using an electronic scale with an accuracy of 0.1 g at 2–3 h intervals, and the horizontal and vertical deformation was also measured. The temperature in the oven was raised to 105 °C once the relative difference between adjacent weights of each sample was less than 0.2%. When the weights of the samples remained unchanged at 105 °C, the samples were considered completely dried and subsequently wetted by the capillary rise method [17]. They were soaked in pure water with the liquid level just below their top for 48 h. The above drying and wetting processes were referred to as a whole drying–wetting cycle. The drying–wetting cycle was repeated, and finally, a total of four cycles were applied.

2.2.3. Deformation Measurement

The horizontal deformation of the sample was captured by a digital camera (Canon EOS60D) and then calculated by employing an image processing technique. Complete details of the image processing technique will be provided in Section 2.3. To ensure consistency across all photographs, the camera and the samples were maintained at fixed positions throughout all cycles; pressing the shutter was substituted with a remote control to avoid the possible slight vibration of the lens caused by pressing. Besides, to eliminate the shadow in photographs that originated from uneven illumination during photographing, the indoor fluorescent lights were turned off; a lamp was hung above the sample as a light source. The vertical deformation was measured by a vernier caliper (accuracy 0.01 mm) at nine defined locations on the soil surface.

2.3. Analysis of Soil Shrinkage and Swelling

2.3.1. Digital Image Processing

The procedure of digital image processing is illustrated in Figure 1. All steps were implemented in batch mode by programmed morphological algorithms in MATLAB R2016a (MathWorks, Boston, USA). First, the round region of interest (diameter 52 mm, inner ring of the top of the cutting ring) was cut out from the original images and resized to a resolution of 1560 × 1560 pixels. Next, the cropped images were converted into grayscale images (grayscale value of the pixels ranges from 0 to 255). From the image, it was apparent that quantifying the horizontal deformation of the soil required the segmentation of the shrinkage zone (zone 1) and the soil matrix (zone 2), and these two zones could be easily identified because of the high contrast, while the four corner zones (zone 3) were useless and had a detrimental effect on threshold segmentation. Therefore, the pixels in zone 3 where the grayscale values approached 255 were removed, and afterwards, a segmentation algorithm named 'OTSU' [42] was employed to determine an appropriate segmentation threshold (*T*). According to the threshold, the grayscale images were transformed into raw binary images. The miscellaneous spots in the raw binary images were cleared by a combination of 'closing' and 'opening' operations. Then, the final binary images for post-calculation were derived. The cross-section area of the soil samples was determined from the proportion of 0 and 1 pixels in the entire image.
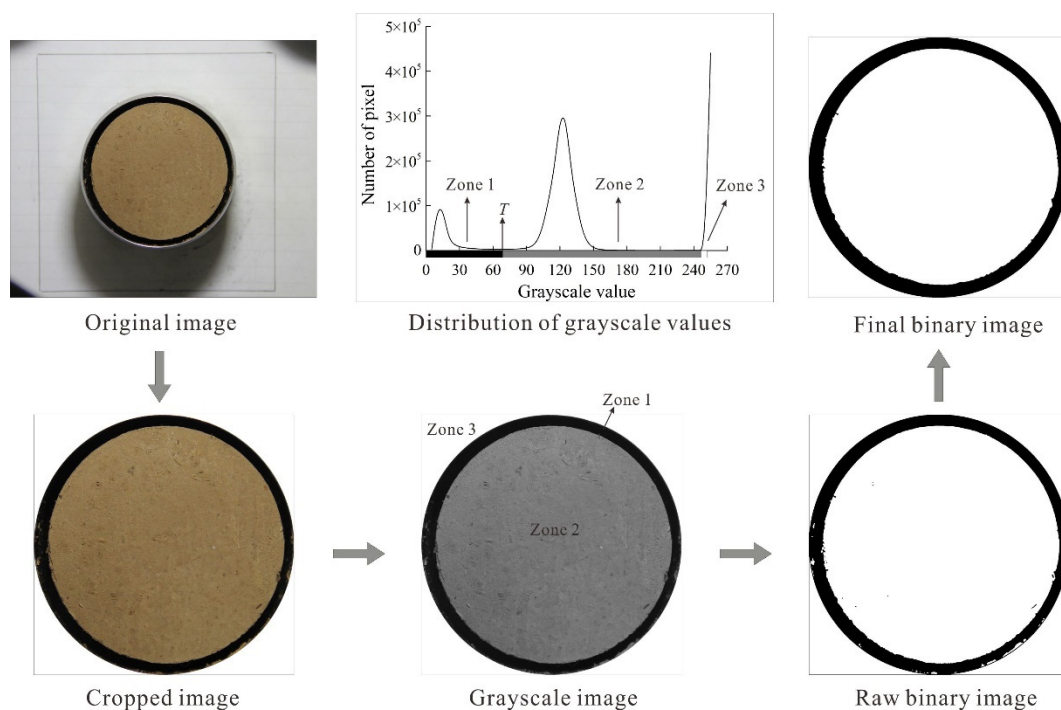

Figure 1. Diagrammatic sketch of digital image processing.

2.3.2. Shrink–Swell Parameters

The parameters used to characterize the soil shrink–swell behavior include horizontal shrinkage potential (ε_{dsk}), vertical shrinkage potential (ε_{zsk}), volume shrinkage potential (ε_{vsk}), horizontal swelling potential (ε_{dsw}), vertical swelling potential (ε_{zsw}) and volume swelling potential (ε_{vsw}). They are calculated as follows:

$$d = (4A/\pi)^{1/2} \tag{1}$$

$$\varepsilon_{dsk} = \left(d_0 - d_f\right)/d_0' \times 100\% \tag{2}$$

$$\varepsilon_{zsk} = \left(z_0 - z_f\right)/z_0' \times 100\% \tag{3}$$

$$\varepsilon_{vsk} = \left(V_0 - V_f \right) / V_0' \times 100\% \tag{4}$$

$$\varepsilon_{dsw} = \left(d_f - d_0 \right) / d_0' \times 100\% \tag{5}$$

$$\varepsilon_{zsw} = \left(z_f - z_0 \right) / z_0' \times 100\% \tag{6}$$

$$\varepsilon_{vsw} = \left(V_f - V_0 \right) / V_0' \times 100\% \tag{7}$$

where d is the equivalent diameter of the soil matrix (mm), A is the cross-sectional area of the soil matrix (mm^2), d_0 and d_f are the initial and final equivalent diameter during a drying or wetting process (mm), respectively, z_0 and z_f are the initial and final height of the soil sample during a drying or wetting process (mm), respectively, V_0 and V_f are the initial and final volume of the soil sample during a drying or wetting process (mm^3), respectively, d_0', z_0' and V_0' are the initial equivalent diameter, height and volume of the soil sample at the beginning of drying during a drying–wetting cycle, respectively. Note that during a drying process $d_0 = d_0'$, $z_0 = z_0'$, $V_0 = V_0'$, while during a wetting process $d_0 \neq d_0'$, $z_0 \neq z_0'$, $V_0 \neq V_0'$.

2.3.3. Soil Shrinkage Curve Model (VG-Peng Model)

The soil shrinkage curve model proposed by Peng and Horn [43] was shown to be suitable for a wide range of soil types [44]. Therefore, the model was adopted in this study. For simplicity, we called the model the VG-Peng model.

$$\begin{cases} e(\vartheta) = e_r + (e_s - e_r) \left[1 + (\chi \vartheta)^{-p} \right]^{-q} & 0 \leq \vartheta \leq \vartheta_s \\ e = V_p / V_s \\ \vartheta = V_w / V_s \end{cases} \tag{8}$$

where e and ϑ are the void ratio and moisture ratio (mm^3 mm^{-3}), respectively, e_s and e_r are the saturated and residual void ratio (mm^3 mm^{-3}), respectively, ϑ_s is the saturated moisture ratio (mm^3 mm^{-3}), χ, p and q are dimensionless fitting parameters, V_p, V_w and V_s are the volumes of the pore, water and solid, respectively (mm^3). Shrinkage zones were separated by the characteristic points of maximum wet-side curvature (ϑ_{shw}, e_{shw}), air entry (ϑ_{ae}, e_{ae}) and shrinkage limit (ϑ_{sl}, e_{sl}). The specific positions of these points on the shrinkage curves were determined by programing in MATLAB R2016a (MathWorks, Boston, MA, USA)

2.3.4. Anisotropy of Soil Deformation

The anisotropy of soil deformation, which characterizes the difference in deformation amplitude between the vertical and horizontal direction, was depicted by the geometry factor (r_s) proposed by Bronswijk. [45].

$$r_s = \ln(V_i / V_0) / \ln(z_i / z_0) \tag{9}$$

where V_0 and V_i are the initial and i^{th} measured volume of soil sample (mm^3), respectively, and z_0 and z_i are the initial and i^{th} measured height of soil sample (mm), respectively. The value of r_s could be divided into five intervals corresponding to five cases of deformation anisotropy. For $r_s = 1$, only vertical deformation can be seen; $1 < r_s < 3$, vertical deformation dominates; $r_s = 3$, only isotropic deformation; $r_s > 3$, horizontal deformation dominates; $r_s \rightarrow \infty$, only horizontal deformation.

2.4. Statistical Analysis

One-way analysis of variance (ANOVA) was employed to assess the effect of drying–wetting cycles on shrinkage–swelling behavior via SPSS version 20.0 (SPSS, Chicago, IL, USA). A least significant difference (LSD) test was applied for comparisons of means at the 0.05 level of significance in terms of the distribution of moisture ratio and void ratio in different shrinkage zones.

3. Results

3.1. Evolution of Soil Size and Shrinkage-Swelling Potential during Cycles

Figure 2a–c display the evolution of soil height, soil equivalent diameter and soil volume during drying–wetting cycles. It was found that the height, equivalent diameter and volume of the soil samples at the end of the drying path increased with the increasing number of drying–wetting cycles. During the first cycle, the height, equivalent diameter and the volume of the samples after drying were around 48 mm, 64 mm and 152,725 mm^3, respectively, while they were increased to about 49 mm, 65 mm and 159,284 mm^3 during the fourth cycle. However, the change of these variables in the wetting path across cycles followed a trend opposite to that in the drying path. They were decreased from 52 mm, 70 mm and 200,119 mm^3 at the end of the wetting path during the first cycle to 51 mm, 68 mm and 183,591 mm^3 during the fourth cycle. The above results showed that the samples lost partial volume after drying–wetting cycles. After wetting, both the height and the equivalent diameter of the samples could not be restored to the initial values before drying. This indicated that the shrinkage and swelling behavior of soil caused by drying–wetting cycles was not completely reversible, and the irreversible deformation occurred in both vertical and horizontal directions.
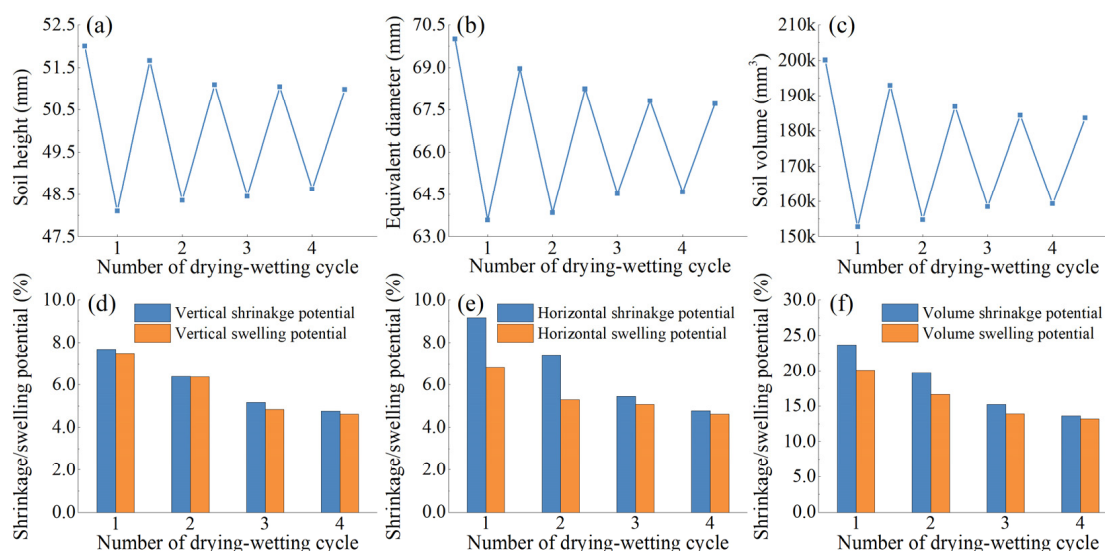

Figure 2. Evolution of soil size and shrinkage–swelling potential during four drying–wetting cycles. (**a**) Soil height; (**b**) Soil equivalent diameter; (**c**) Soil volume; (**d**) Vertical shrinkage/swelling potential; (**e**) Horizontal shrinkage/swelling potential; (**f**) Volume shrinkage/swelling potential.

Figure 2d–f show the variation of the soil shrinkage and swelling potential during cycles. It was observed that all potentials shared similar trends throughout four cycles. Specifically, they decreased with the sequence of cycles, and the differences between the third and fourth cycles were relatively small, suggesting that with the increasing generation of drying–wetting cycles, the ability of soil deformation was weakening, and the soil structure became more stable [46]. For individual cycles, the shrinkage potential was larger than the swelling potential in both vertical and horizontal directions. The difference between shrinkage potential and swelling potential indicated the irreversible deformation [31]. Accordingly, the irreversible deformation of these soil samples ranged from 0.34% to 0.13% in the vertical direction, from 1.48% to 0.15% in the horizontal direction, from 3.58% to 0.43% in volume, and in general, they exhibited decreasing trends with repeated drying–wetting cycles.

3.2. Dynamics of Soil Height and Equivalent Diameter during Drying

The dynamics of soil height and soil equivalent diameter during four drying paths are presented in Figure 3. The soil height decreased with the decreasing soil water content for

all drying paths. Two distinct stages could be roughly identified according to the variation of decreasing rate: a declining stage during which the soil height declined rapidly and almost linearly as the soil water content decreased from the saturated water content to about 0.15 g g^{-1}; and a subsequent residual stage during which the soil height decreased slowly until the end of drying. The dynamic change of soil equivalent diameter during a single drying path could be divided into three stages: constant stage, declining stage and residual stage. At the constant stage, the equivalent diameter did not change or only decreased slightly, although the soil water content decreased. The declining stage and the residual stage were similar to those of the dynamics of soil height. The existence of the constant stage manifested that during drying, vertical and horizontal shrinkage were not synchronized. Vertical shrinkage preceded horizontal shrinkage at the beginning of drying. Besides, it was observed that the saturated soil water content was decreasing with increasing cycles. During the first drying cycle, the saturated water content was around 0.38 g g^{-1}, while during the last two cycles, the saturated water content dropped to about 0.34 g g^{-1}, which implied a decrease in soil porosity after repeated drying–wetting cycles.
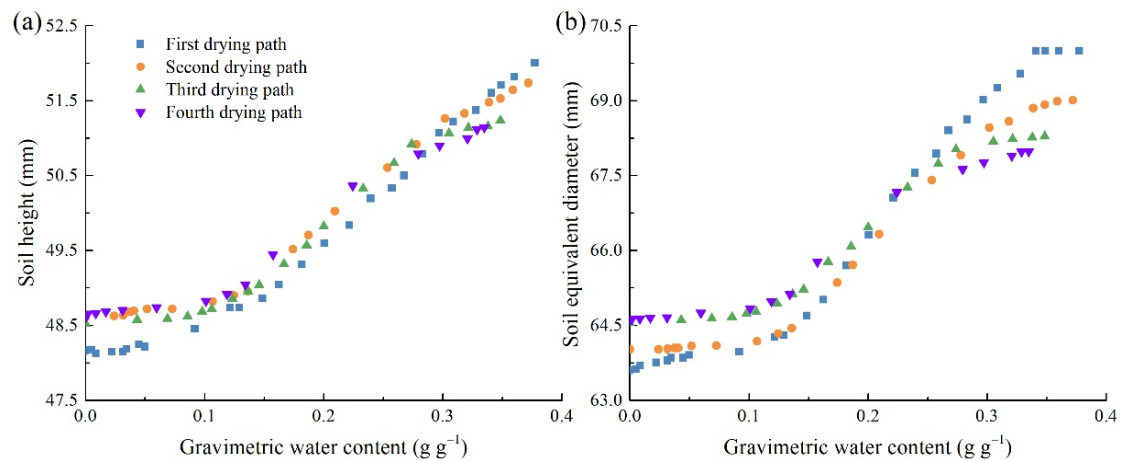

Figure 3. Dynamics of soil height and equivalent diameter during four drying paths. For brevity, only the data of replicate 1 are presented. (**a**) Soil height; (**b**) Soil equivalent diameter.

3.3. Changes of Soil Shrinkage Curve, Shrinkage Zones

Soil shrinkage curves during four drying paths are displayed in Figure 4. The corresponding fitting parameters and goodness of fit (root mean square error *RMSE*, Nash–Sutcliffe model efficiency coefficient *NSE*, coefficient of determination R^2) of the VG-Peng model are shown in Table 1. Fitting was accomplished by minimizing the sum of squared errors by using the curve fitting tool in MATLAB R2016a (MathWorks, USA). Since e_r and e_s were derived from the experiment, they were inputted as known parameters during fitting. For all samples during different drying paths, the values of *RMSE* are nearly 0.01; meanwhile, the values of *NSE* and R^2 are close to 1.0, verifying that the VG-Peng model is suitable for fitting soil shrinkage curves. It was observed that all shrinkage curves did not start from the 1:1 line as expected, which was likely because the soil samples could not be thoroughly saturated by the capillary rise method. A decreasing trend of e_s with increasing drying paths was observed, whereas a slightly increasing trend was observed in e_r, indicating a reduction in both soil volume and soil shrinkage capacity after drying–wetting cycles.
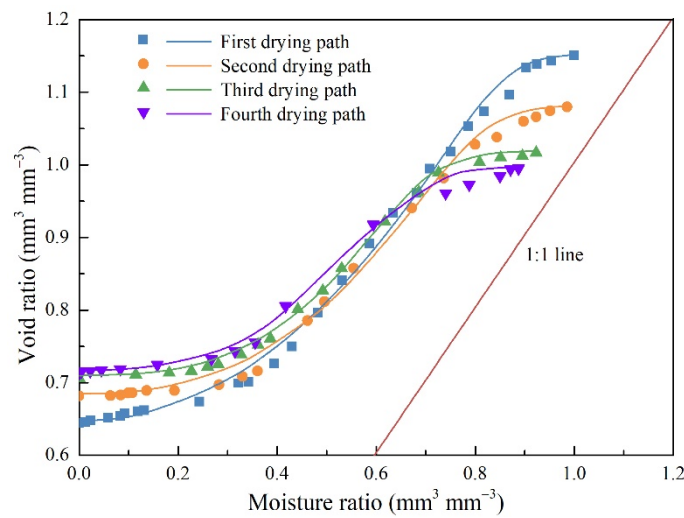
Figure 4. Soil shrinkage curves during four drying paths. Scatters are measured values, and lines were fit using Equation (8). For brevity, only the data of replicate 1 are presented.

Table 1. Parameters and goodness of fit of the VG-Peng model for samples during four drying paths.

Drying Path	Replicate	e_r	e_s	χ	p	q	RMSE *	NSE *	R^2 *
First	1	0.644	1.151	1.165	20.572	0.102	0.011	0.997	0.997
	2	0.662	1.164	1.149	18.232	0.110	0.011	0.996	0.997
	3	0.612	1.126	1.166	23.662	0.085	0.011	0.997	0.997
Second	1	0.681	1.080	1.238	16.658	0.148	0.010	0.996	0.997
	2	0.671	1.076	1.245	16.137	0.136	0.009	0.997	0.997
	3	0.632	1.056	1.218	22.353	0.098	0.012	0.995	0.995
Third	1	0.706	1.016	1.435	14.908	0.188	0.005	0.998	0.999
	2	0.705	1.004	1.421	12.793	0.189	0.005	0.998	0.999
	3	0.689	0.996	1.520	11.354	0.231	0.009	0.994	0.995
Fourth	1	0.714	0.995	1.529	12.387	0.229	0.008	0.995	0.996
	2	0.718	0.992	1.423	14.053	0.177	0.009	0.994	0.996
	3	0.697	0.949	1.471	14.907	0.178	0.007	0.996	0.998

* *RMSE*, *NSE* and R^2 refer to the root mean square error, Nash–Sutcliffe model efficiency coefficient and coefficient of determination, respectively.

The distribution of moisture ratio and void ratio in different soil shrinkage zones during four drying paths are displayed in Figure 5. During the four drying paths, all the shrinkage curves had four complete shrinkage zones: structural shrinkage, proportional shrinkage, residual shrinkage and zero shrinkage. However, there were appreciable differences in the distribution of moisture ratio and void ratio in shrinkage zones across different drying paths. With respect to moisture ratio, it was evident that during the first and second drying path, the proportional and residual shrinkage zone had the highest moisture ratio, both of which accounted for more than 30% of the total water loss, indicating that these two zones dominated the soil moisture variation. In particular, during the first drying cycle, the moisture ratio within the proportional shrinkage zone was 0.49 cm^3 cm^{-3} which was almost half of the total change of moisture ratio. However, with the increasing number of drying–wetting cycles, the moisture ratio within these two zones was significantly reduced. During the third and fourth drying cycle, the moisture ratio within the two zones was close to 0.22 cm^3 cm^{-3}. By contrast, the other two zones, the structural and zero shrinkage zone, gradually played important roles in water loss. Between the second and third drying paths, the decrease in moisture ratio within the proportional and residual shrinkage zone and the increase within the structural and zero shrinkage zone reached the significance level. With regard to the distribution of the void ratio, the proportional shrinkage zone occupied

the most void ratios across all cycles, indicating that this shrinkage zone dominated the soil deformation, although the void ratio within the proportional shrinkage zone sharply decreased as the cycles proceeded, and during the last drying cycle, the ratio approached 0.15 cm^3 cm^{-3}. The void ratio within the structural shrinkage zone almost remained unchanged at around 0.02 mm^3 mm^{-3} across cycles. The ratio within the residual shrinkage zone and zero shrinkage zone, respectively, exhibited a slight downward and upward tendency with the repeated cycles. It was worth noting that the distribution of moisture ratio and void ratio in the shrinkage zones during the last two cycles were not significantly different at the significance level of 0.05, implying that the soil samples nearly reached an equilibrium state after three drying–wetting cycles.
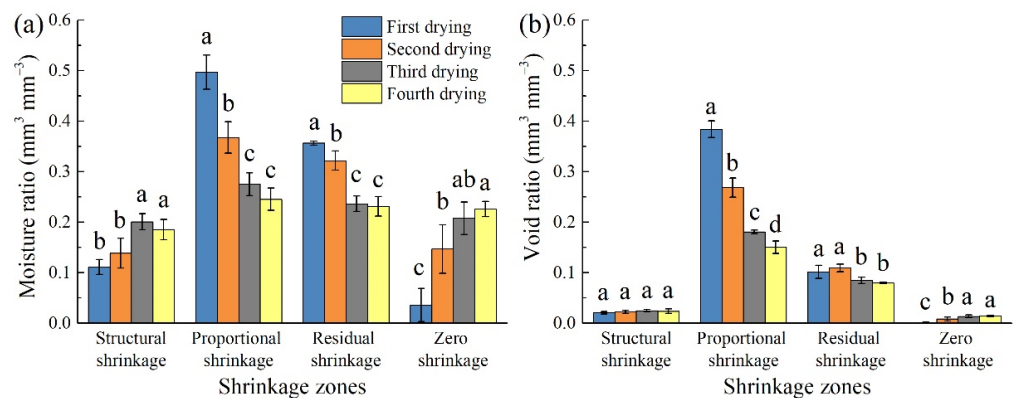

Figure 5. Distribution of moisture ratio (**a**) and void ratio (**b**) in different soil shrinkage zones. For the same shrinkage zones, moisture ratio, void ratio and average slope labelled with different letters across different drying paths are significantly different at the significance level of 0.05.

3.4. Variation of Geometry Factor during Cycles

The variation of the shrinkage geometry factor with decreasing soil water content is displayed in Figure 6. For all drying paths, the shrinkage geometry factor exhibited similar trends. At the beginning of drying, the shrinkage geometry factor was close to or slightly larger than 1.0, indicating that vertical shrinkage was overwhelmingly dominant while horizontal shrinkage was negligible at the outset of drying. Subsequently, the shrinkage geometry factor steeply increased, suggesting a fast increase in horizontal shrinkage. When the soil water content approximately decreased to around 0.20 g g^{-1}, the shrinkage geometry factor entered a relatively stable plateau where its value was generally fluctuating between 3.0–3.5 until the end of drying.
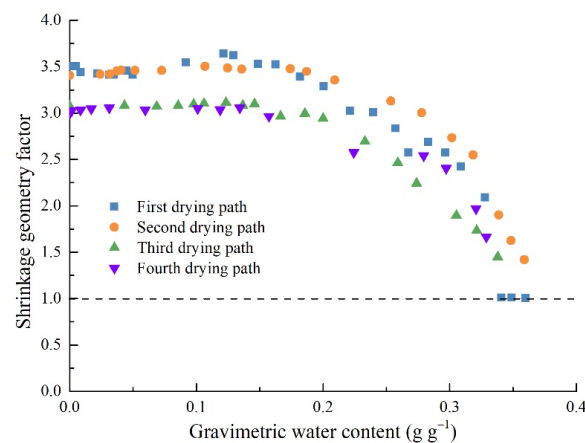

Figure 6. Variation of shrinkage geometry factor with decreasing soil water content during four drying paths. For brevity, only the data of replicate 1 are presented.

4. Discussion

4.1. Irreversible Deformation during Drying–Wetting Cycles

Irreversible deformation of soil was clearly observed in this experiment. The swelling amount during wetting was smaller than the shrinkage amount during drying for individual drying–wetting cycles, giving rise to a loss of soil volume. Similar phenomena were observed in many other experimental studies [34,47,48]. There are two main reasons accounting for irreversible deformation (shrinkage accumulation in our experiment). One is that the soil samples were not thoroughly saturated after wetting as indicated in Figure 4. The other is the intrinsic properties of soil structure. Generally, it is considered that soil pores have a double-level structure: microstructure and macrostructure [10,29], respectively, corresponding to inter-aggregate and intra-aggregate pores [49,50]. When water input was not intense, water would preferentially move through soil aggregates [51]. Accordingly, in our experiment, the water entered the intra-aggregate pores first during the capillary wetting process, leading to swelling of the aggregates. For stable aggregates, the deformation during drying and wetting displayed relatively good reversibility [46]. However, there were a considerable number of unstable aggregates in the soil during the early cycles. As the swelling proceeded, the stability of the unstable aggregates was gradually decreased [52], eventually leading to their disintegration into smaller sized ones, accompanied by the rearrangement of aggregates [41]. The disintegration and rearrangement of the unstable aggregates appreciably modified not only the microstructure but also the macrostructure of soil, causing irreversible deformation since the realignment of macrostructure which determined soil granular skeleton was found to be irreversible during drying and wetting [38]. Irreversible deformation of soil can result in shrinkage accumulation or swelling accumulation, which is mainly dependent on the initial bulk density of soil. The former case tends to be found in soil with low bulk densities, while the latter case is prone to occur in loose soil [10]. This explains the shrinkage accumulation (volume loss) during the early cycles observed in our experiment.

It was also observed that the magnitude of volume loss reduced sharply with the increasing number of drying–wetting cycles. During the last two cycles, the irreversible deformation was negligible, so the soil shrinkage and swelling during drying and wetting could even be regarded as reversible, which is consistent with the observations in other studies [24,37]. This was because the unstable aggregates in soil had almost disappeared and were transformed into stable ones after several drying–wetting cycles. During subsequent cycles, soil deformation only originated from the reversible deformation of the aggregates (microstructure), and no rearrangement or slippage of aggregates that could change the macrostructure occurred [46].

Soil shrinkage and swelling behavior is essentially the shift of soil porosity between inside and outside soil aggregates [53], which is macroscopically performed as the generation or closure of soil cracks in the horizontal direction and subsidence or heave of soil in the vertical direction. The shrinkage accumulation in our experiment caused the permanent detachment of the soil matrix from the wall of cutting rings throughout all cycles. It can thus be deduced that without the impact of large external forces, many desiccation cracks in the loose soil of farmland form due to previous shrinkage accumulation rather than current drying, and they are likely to persistently exist even if the soil water content is relatively very high, which inevitably complicates the hydrological process in farmland. Besides, it is reasonable to infer that for a given soil in farmland, there are appropriate soil bulk densities, under which the shrinkage accumulation can be limited and hence the number and size of soil desiccation cracks can be markedly reduced.

4.2. Effect of Drying–Wetting Cycles on Shrinkage Curve, Shrinkage Zones

Soil shrinkage curves can provide detailed information on soil pore structure [54]. Apparent changes of soil shrinkage curves across different drying paths were observed in our study, indicating that drying–wetting cycles had a marked influence on soil pore structure. With the increasing number of drying–wetting cycles, the saturated void ratio

progressively decreased from 1.15 to 1.00, revealing the decrease of soil porosity with cycles, which was attributed to the shrinkage accumulation. The difference between the saturated and residual void ratio was also reduced with the sequence of drying–wetting cycles, showing the diminishing shrinkage capacity of the soil.

Regarding the shrinkage zones, it was found that during all drying paths, the soil had four complete zones. Figure 7 present the simplified shrinkage process of soil during drying. When the initially saturated soil was under drying conditions (Figure 7a), water in inter-aggregate pores was lost from the soil surface by evaporation or drained from the bottom by gravity (not shown in Figure 7). Soil subsidence occurred, and the water–air meniscus formed in soil (Figure 7b), causing capillary suction and thus tensile stress among aggregates [2,11]. The tensile stress increased as the meniscus became more curved due to further water loss, and when it reached large values, which we called critical tensile stress, the soil aggregates were driven significantly closer to each other. The process before the critical tensile stress was reached was structural shrinkage. After that, the soil shrinkage entered proportional shrinkage, and the soil shrank rapidly, mainly originating from the deformation of the soil skeleton (Figure 7c). As evaporation proceeded, the meniscus developed inside the soil and gradually evolved into a liquid bridge between aggregates which continued pulling the aggregates closer (Figure 7d). After the rupture of liquid bridges (Figure 7e), the shrinkage velocity significantly slowed down, and the soil shrinkage reached residual shrinkage, during which the water was mainly evaporated from the intra-aggregate pores, and the soil shrinkage primarily resulted from the volume decrease of aggregates (Figure 7f). As the drying continued, the water loss in intra-aggregate pores no longer caused the volume change of aggregates, at which point the soil shrinkage entered zero shrinkage (Figure 7g).
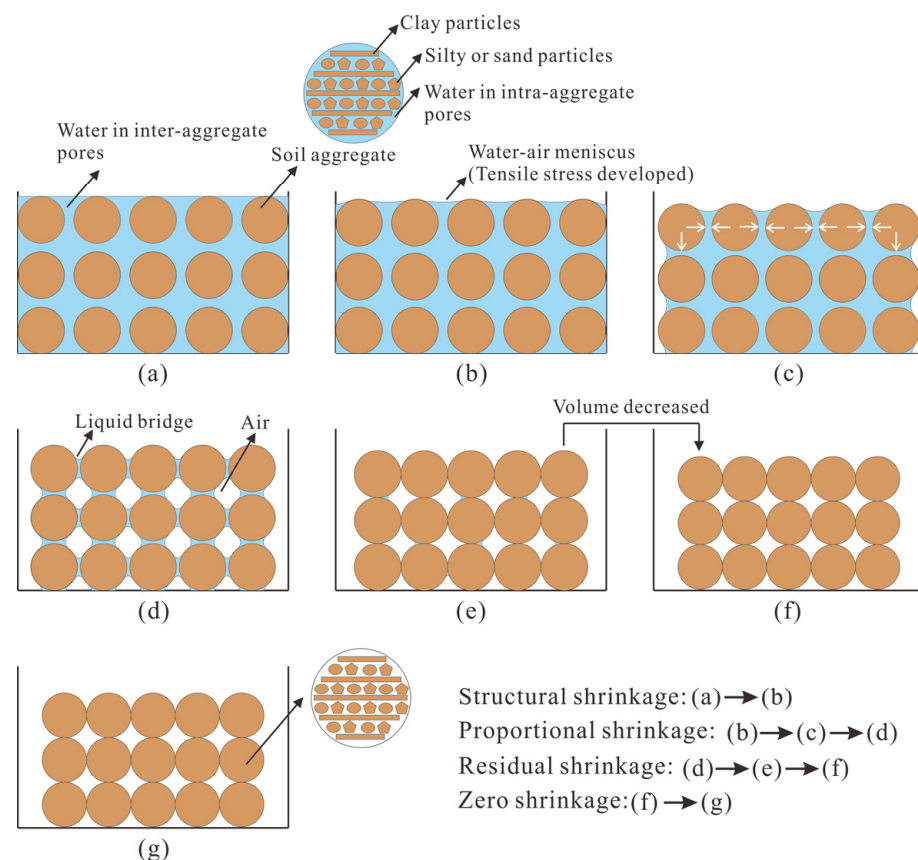

Figure 7. Schematic drawings of simplified soil shrinkage process. (**a**–**g**) present different states of soil sample during structural, proportional, residual and zero shrinkage.

With respect to the variation of the distribution of moisture ratio and void ratio in shrinkage zones between cycles, it was found that although there were no new root holes, biopores and cracks observed inside the samples during the experiment, the moisture ratio within the structural shrinkage zone increased with the increasing number of drying–wetting cycles (Figure 5a). This was likely because the soil structure became more stable with increased cycles. Drying–wetting cycles induced the breakdown, rearrangement and reorientation of aggregates, gradually promoting the stability of soil structure [37,55], thereby increasing the value of critical tensile stress. Another possible explanation was that drying–wetting cycles may have induced microcracks in the soil. These microcracks could neither be clearly identified by visual inspection nor captured by the camera due to the limit of the resolution. A significant decrease was observed in the moisture ratio within the proportional and residual shrinkage zones with the increasing number of drying–wetting cycles, indicating that the shrinkage accumulation observed during the cycles essentially originated from the decrease in void volume within these two zones. Additionally, it was observed that the void ratio within the proportional shrinkage zone was steeply reduced with increased cycles, which meant that the diminishing shrinkage capacity of the soil was due in large part to the change in the proportional shrinkage zone. Nevertheless, the void ratio within the proportional shrinkage zone was still obviously larger than that within other zones, indicating that most shrinkage occurred in the proportional shrinkage zone. This is in line with the findings of previous studies [17,24,54]. Though drying–wetting cycles had an important impact on soil shrinkage behavior, it was found that with the increasing number of drying–wetting cycles, the difference in soil porosity, soil shrinkage curves and shrinkage zones between adjacent cycles was apparently decreased. This was because the soil structure became more stable with increased cycles and the soil nearly reached an equilibrium state after three cycles.

4.3. Anisotropy of Soil Deformation

As can be seen in Figure 6, upon drying, the shrinkage geometry factor started at about 1.0, then increased rapidly and gradually stabilized at around 3.0, indicating that at the beginning of drying, there was only vertical shrinkage and almost no horizontal shrinkage. Subsequently, horizontal shrinkage increased, but vertical shrinkage still dominated the soil deformation; then as horizontal shrinkage continued growing, horizontal shrinkage became close to vertical shrinkage until the end of drying. Figure 8 present the correspondence among the evolution of soil height, equivalent diameter, soil shrinkage curve and shrinkage geometry factor during drying. During the drying process, soil shrinkage firstly entered the structural shrinkage. The water loss did not generate sufficient capillary suction thus the diameter almost remained constant, and the variation of soil equivalent diameter was at the constant stage. However, due to the effect of gravity, water was lost from large inter-aggregate pores, and soil subsidence occurred [56]. The variation of soil height entered the declining stage immediately after the drying began. Therefore, at the initial time of drying, vertical shrinkage almost completely dominated the soil deformation. During proportional shrinkage, the effect of gravity on vertical shrinkage diminished. The soil aggregates were drawn closer to each other in both vertical and horizontal directions by the tensile stress, constantly narrowing the gap between the contribution of vertical and horizontal shrinkage to soil deformation and eventually leading to very close horizontal and vertical shrinkage (shrinkage geometry factor was near 3.0). Next, during residual and zero shrinkage, water was mainly evaporated from the intra-aggregate pores, which did not cause an obvious difference between horizontal and vertical shrinkage. Therefore, the shrinkage geometry factor became generally stable after proportional shrinkage.
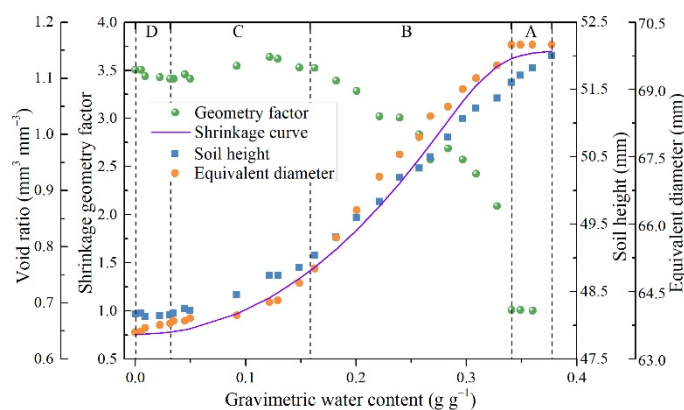
Figure 8. Correspondence among the evolution of soil height, equivalent diameter, soil shrinkage curve and shrinkage geometry factor during drying. A, B, C and D represent structural, proportional, residual and zero shrinkage zones, respectively. For brevity, only the data of replicate 1 during the first drying path are presented.

5. Conclusions

This study investigated the impact of drying–wetting cycles on the shrink–swell behavior of clay loam in farmland. The results showed that the soil size (height, equivalent diameter and volume) and the shrinkage–swelling potential decreased with repeated drying–wetting cycles, and the shrinkage potential was larger than the swelling potential within the same cycles, indicating the irreversible deformation (shrinkage accumulation) of the soil, and thereby suggesting that the existence of partial cracks in farmland was probably due to previous drying rather than current drying. During drying paths, the variation of soil height could be divided into a declining stage and residual stage, while the variation of equivalent diameter consisted of three stages: constant stage, declining stage and residual stage. The VG-Peng model was proven to fit soil shrinkage curves very well. All the shrinkage curves had four complete shrinkage zones during four cycles, but the distribution of moisture ratio and void ratio in the four zones altered significantly across cycles, indicating that the drying–wetting cycles had appreciable effects on the soil pore structure. As the cycle progressed, the void ratio and moisture ratio decreased the most in the proportional shrinkage zone. Nevertheless, the proportional shrinkage zone covered most of the volume change in contrast to the other three zones. The impact of drying–wetting cycles on soil's shrink–swell behavior weakened with the increasing number of cycles. After three cycles, the soil nearly reached an equilibrium state as the differences in shrinkage and swelling characteristic between cycles became minimal. Due to the effect of gravity, vertical shrinkage dominated deformation at the early stage of drying, but after entering residual shrinkage, the shrinkage deformation was nearly isotropic.

Data Availability Statement: The data that support this study cannot be publicly shared due to ethical or privacy reasons and may be shared upon reasonable request to the corresponding author if appropriate.

Conflicts of Interest: The authors declare no conflict of interest.

References

1. Wen, T.; Wang, P.; Shao, L.; Guo, X. Experimental investigations of soil shrinkage characteristics and their effects on the soil water characteristic curve. *Eng. Geol.* **2021**, *284*, 106035. [CrossRef]
2. Tang, C.S.; Shi, B.; Liu, C.; Suo, W.B.; Gao, L. Experimental characterization of shrinkage and desiccation cracking in thin clay layer. *Appl. Clay Sci.* **2011**, *52*, 69–77. [CrossRef]
3. Li, H.D.; Tang, C.S.; Cheng, Q.; Li, S.J.; Gong, X.P.; Shi, B. Tensile strength of clayey soil and the strain analysis based on image processing techniques. *Eng. Geol.* **2019**, *253*, 137–148. [CrossRef]
4. Zeng, H.; Tang, C.S.; Cheng, Q.; Zhu, C.; Yin, L.Y.; Shi, B. Drought-induced soil desiccation cracking behavior with consideration of basal friction and layer thickness. *Water Resour. Res.* **2020**, *56*, e2019WR026948. [CrossRef]
5. Zhang, J.M.; Luo, Y.; Zhou, Z.; Chong, L.; Victor, C.; Zhang, Y.F. Effects of preferential flow induced by desiccation cracks on slope stability. *Eng. Geol.* **2021**, *288*, 106164. [CrossRef]
6. Xing, X.; Li, Y.; Ma, X. Water retention curve correction using changes in bulk density during data collection. *Eng. Geol.* **2018**, *233*, 231–237. [CrossRef]
7. Greve, A.; Andersen, M.S.; Acworth, R.I. Investigations of soil cracking and preferential flow in a weighing lysimeter filled with cracking clay soil. *J. Hydrol.* **2010**, *393*, 105–113. [CrossRef]
8. Haque, A.N.A.; Uddin, M.K.; Sulaiman, M.F.; Amin, A.M.; Hossain, M.; Solaiman, Z.M.; Mosharrof, M. Biochar with alternate wetting and drying irrigation: A potential technique for paddy soil management. *Agriculture* **2021**, *11*, 367. [CrossRef]
9. Paul, P.L.C.; Bell, R.W.; Barrett-Lennard, E.G.; Kabir, E. Impact of rice straw mulch on soil physical properties, sunflower root distribution and yield in a salt-affected clay-textured soil. *Agriculture* **2021**, *11*, 264. [CrossRef]
10. Wang, G.; Wei, X. Modeling swelling–shrinkage behavior of compacted expansive soils during wetting–drying cycles. *Can. Geotech. J.* **2015**, *52*, 783–794. [CrossRef]
11. Qi, W.; Zhang, Z.Y.; Wang, C. Desiccation and cracking behaviour of clay loam subjected to different irrigation methods during wetting-drying cycles. *Eur. J. Soil Sci.* **2020**, *72*, 793–809. [CrossRef]
12. Grossman, R.; Brasher, B.; Franzmeier, D.; Walker, J.L. Linear extensibility as calculated from natural-clod bulk density measurements1. *Soil Sci. Soc. Am. J.* **1968**, *32*, 570–573. [CrossRef]
13. Klopp, H.W.; Arriaga, F.J.; Likos, W.J.; Bleam, W.F. Atterberg limits and shrink/swell capacity of soil as indicators for sodium sensitivity within a gradient of soil exchangeable sodium percentage and salinity. *Geoderma* **2019**, *353*, 449–458. [CrossRef]
14. Valle, S.R.; Dörner, J.; Zúñiga, F.; Dec, D. Seasonal dynamics of the physical quality of volcanic ash soils under different land uses in southern Chile. *Soil Tillage Res.* **2018**, *182*, 25–34. [CrossRef]
15. Deng, C.; Teng, X.; Peng, X.; Zhang, B. Effects of simulated puddling intensity and pre-drying on shrinkage capacity of a paddy soil under long-term fertilization. *Soil Tillage Res.* **2014**, *140*, 135–143. [CrossRef]
16. Dinka, T.M.; Morgan, C.L.S.; McInnes, K.J.; Kishné, A.S.; Daren Harmel, R. Shrink–swell behavior of soil across a Vertisol catena. *J. Hydrol.* **2013**, *476*, 352–359. [CrossRef]
17. Peng, X.H.; Horn, R. Anisotropic shrinkage and swelling of some organic and inorganic soils. *Eur. J. Soil Sci.* **2007**, *58*, 98–107. [CrossRef]
18. Groenevelt, P.H.; Grant, C.D. Re-evaluation of the structural properties of some British swelling soils. *Eur. J. Soil Sci.* **2001**, *52*, 469–477. [CrossRef]
19. McGarry, D.; Malafant, K.W.J. The analysis of volume change in unconfined units of soil. *Soil Sci. Soc. Am. J.* **1987**, *51*, 290–297. [CrossRef]
20. Amenuvor, A.C.; Li, G.; Wu, J.; Hou, Y.; Chen, W. An image-based method for quick measurement of the soil shrinkage characteristics curve of soil slurry. *Geoderma* **2020**, *363*, 114165. [CrossRef]
21. Shao, M.; Lv, D. Experimental study on soil shrinkage characteristic curves. *Acta Pedol. Sin.* **2003**, *40*, 471–474.
22. Tariq, A.-u.-R.; Durnford, D.S. Analytical volume change model for swelling clay soils. *Soil Sci. Soc. Am. J.* **1993**, *57*, 1183–1187. [CrossRef]
23. Braudeau, E.; Costantini, J.M.; Bellier, G.; Colleuille, H. New device and method for soil shrinkage curve measurement and characterization. *Soil Sci. Soc. Am. J.* **1999**, *63*, 525–535. [CrossRef]
24. Estabragh, A.R.; Parsaei, B.; Javadi, A.A. Laboratory investigation of the effect of cyclic wetting and drying on the behaviour of an expansive soil. *Soils Found.* **2015**, *55*, 304–314. [CrossRef]
25. Jong, E.D.; Kozak, L.M.; Storehouse, H.B. Comparison of shrink-swell indices of some Saskatchewan soils and their relationships to standard soil. *Can. J. Soil Sci.* **1992**, *72*, 429–439. [CrossRef]
26. Gray, C.W.; Allbrook, R. Relationships between shrinkage indices and soil properties in some New Zealand soils. *Geoderma* **2002**, *108*, 287–299. [CrossRef]

27. Nowamooz, H.; Jahangir, E.; Masrouri, F. Volume change behaviour of a swelling soil compacted at different initial states. *Eng. Geol.* **2013**, *153*, 25–34. [CrossRef]

28. Zhang, Z.B.; Peng, X.; Wang, L.L.; Zhao, Q.G.; Lin, H. Temporal changes in shrinkage behavior of two paddy soils under alternative flooding and drying cycles and its consequence on percolation. *Geoderma* **2013**, *192*, 12–20. [CrossRef]

29. Nowamooz, H.; Masrouri, F. Hydromechanical behaviour of an expansive bentonite/silt mixture in cyclic suction-controlled drying and wetting tests. *Eng. Geol.* **2008**, *101*, 154–164. [CrossRef]

30. Monroy, R.; Zdravkovic, L.; Ridley, A. Evolution of microstructure in compacted London Clay during wetting and loading. *Géotechnique* **2010**, *60*, 105–119. [CrossRef]

31. Shahsavani, S.; Vakili, A.H.; Mokhberi, M. The effect of wetting and drying cycles on the swelling-shrinkage behavior of the expansive soils improved by nanosilica and industrial waste. *Bull. Eng. Geol. Environ.* **2020**, *79*, 4765–4781. [CrossRef]

32. Xing, X.; Ma, X. Analysis of cracking potential and modification of soil-water characteristic curve by adding wheat residues. *Soil Sci. Soc. Am. J.* **2019**, *83*, 1299–1308. [CrossRef]

33. Estabragh, A.R.; Moghadas, M.; Javadi, A.A. Effect of different types of wetting fluids on the behaviour of expansive soil during wetting and drying. *Soils Found.* **2013**, *53*, 617–627. [CrossRef]

34. Peng, X.H.; Horn, R.; Smucker, A. Pore shrinkage dependency of inorganic and organic soils on wetting and drying cycles. *Soil Sci. Soc. Am. J.* **2007**, *71*, 1095–1104. [CrossRef]

35. Zhao, G.T.; Zou, W.L.; Han, Z.; Wang, D.X.; Wang, X.Q. Evolution of soil-water and shrinkage characteristics of an expansive clay during freeze-thaw and drying-wetting cycles. *Cold Reg. Sci. Technol.* **2021**, *186*, 103275. [CrossRef]

36. Aksakal, E.L.; Angin, I.; Sari, S. Effects of freeze-thaw cycles on consistency limits of soils amended with diatomite. *Soil Tillage Res.* **2021**, *213*, 105144. [CrossRef]

37. Yazdandoust, F.; Yasrobi, S.S. Effect of cyclic wetting and drying on swelling behavior of polymer-stabilized expansive clays. *Appl. Clay Sci.* **2010**, *50*, 461–468. [CrossRef]

38. Sun, H.; Mašín, D.; Najser, J.; Neděla, V.; Navrátilová, E. Bentonite microstructure and saturation evolution in wetting–drying cycles evaluated using ESEM, MIP and WRC measurements. *Géotechnique* **2019**, *69*, 713–726. [CrossRef]

39. She, D.L.; Sun, X.Q.; Gamareldawla, A.H.D.; Nazar, E.A.; Hu, W.; Edith, K.; Yu, S.E. Benefits of soil biochar amendments to tomato growth under saline water irrigation. *Sci. Rep.* **2018**, *8*, 14743. [CrossRef]

40. Liu, M.; Wang, S.; Fan, J.; Fu, W.; Du, M. Rapid in-situ determination of soil evaporation with cutting ring method. *Chin. J. Soil Sci.* **2021**, *52*, 55–61.

41. Pires, L.F.; Bacchi, O.O.S.; Reichardt, K. Gamma ray computed tomography to evaluate wetting/drying soil structure changes. *Nucl. Instrum. Methods Phys. Res. Sect. B Beam Interact. Mater. At.* **2005**, *229*, 443–456. [CrossRef]

42. Otsu, N. A threshold selection method from gray-level histograms. *IEEE Trans. Syst. Man Cybern. Syst.* **1979**, *9*, 62–66. [CrossRef]

43. Peng, X.H.; Horn, R. Modeling soil shrinkage curve across a wide range of soil types. *Soil Sci. Soc. Am. J.* **2005**, *69*, 584–592. [CrossRef]

44. Peng, X.H.; Horn, R. Identifying six types of soil shrinkage curves from a large set of experimental data. *Soil Sci. Soc. Am. J.* **2013**, *77*, 372. [CrossRef]

45. Bronswijk, J.J.B. Shrinkage geometry of a heavy clay soil at various stress. *Soil Sci. Soc. Am. J.* **1990**, *54*, 1500–1502. [CrossRef]

46. Airò Farulla, C.; Ferrari, A.; Romero, E. Volume change behaviour of a compacted scaly clay during cyclic suction changes. *Can. Geotech. J.* **2010**, *47*, 688–703. [CrossRef]

47. Wang, C.; Zhang, Z.Y.; Qi, W.; Fan, S.M. Morphological approach to quantifying soil cracks: Application to dynamic crack patterns during wetting-drying cycles. *Soil Sci. Soc. Am. J.* **2018**, *82*, 751–771. [CrossRef]

48. Mawlood, Y.I.; Hummadi, R.A. Reversible and irreversible deformations of expansive clays. *Proc. Inst. Civ. Eng. Geotech. Eng.* **2019**, *172*, 442–452. [CrossRef]

49. Abou Najm, M.R.; Jabro, J.D.; Iversen, W.M.; Mohtar, R.H.; Evans, R.G. New method for the characterization of three-dimensional preferential flow paths in the field. *Water Resour. Res.* **2010**, *46*. [CrossRef]

50. Qi, W.; Zhang, Z.Y.; Wang, C.; Chen, Y.; Zhang, Z.M. Crack closure and flow regimes in cracked clay loam subjected to different irrigation methods. *Geoderma* **2020**, *358*, 113978. [CrossRef]

51. Carminati, A.; Kaestner, A.; Lehmann, P.; Flühler, H. Unsaturated water flow across soil aggregate contacts. *Adv. Water Resour.* **2008**, *31*, 1221–1232. [CrossRef]

52. Ma, R.; Cai, C.; Li, Z.; Wang, J.; Xiao, T.; Peng, G.; Yang, W. Evaluation of soil aggregate microstructure and stability under wetting and drying cycles in two Ultisols using synchrotron-based X-ray micro-computed tomography. *Soil Tillage Res.* **2015**, *149*, 1–11. [CrossRef]

53. Stewart, R.D.; Rupp, D.E.; Abou Najm, M.R.; Selker, J.S. A unified model for soil shrinkage, subsidence, and cracking. *Vadose Zone J.* **2016**, *15*. [CrossRef]

54. Fang, H.; Zhang, Z.; Li, D.; Liu, K.; Zhang, K.; Zhang, W.; Peng, X.; Zhou, H. Temporal dynamics of paddy soil structure as affected by different fertilization strategies investigated with soil shrinkage curve. *Soil Tillage Res.* **2019**, *187*, 102–109. [CrossRef]

55. Zemenu, G.; Martine, A.; Roger, C. Analysis of the behaviour of a natural expansive soil under cyclic drying and wetting. *Bull. Eng. Geol. Environ.* **2009**, *68*, 421–436. [CrossRef]

56. Wang, C.; Zhang, Z.; Cao, D.; Chen, Y.; Qi, W.; Ma, L. Crack porosity estimation model based on VG-PENG shrinkage characteristic curve and soil shrinkage anisotropy. *Trans. Chin. Soc. Agric. Eng.* **2021**, *37*, 112–121.